6th European Conference on Computational Mechanics (ECCM 6)
7th European Conference on Computational Fluid Dynamics (ECFD 7)
11-15 June 2018, Glasgow, UK

EFFICIENCY OF THE FAST MULTIPOLE BEM WITH QUADRATIC ELEMENTS FOR 3D LINEAR ELASTICITY

JACEK PTASZNY[1], PAWEŁ SWINKA[2]

[1] Institute of Computational Mechanics and Engineering
Silesian University of Technology, Konarskiego 18A, 44-100 Gliwice, Poland
jacek.ptaszny@polsl.pl, www.icme.polsl.pl

[2] Graduate Student, Faculty of Mechanical Engineering
Silesian University of Technology Konarskiego 18A, 44-100 Gliwice, Poland
pawel.swinka@gmail.com

Key words: 3D Elasticity, Fast Multipole Boundary Element Method, Quadratic Elements, Efficiency, Finite Element Method

Abstract. A Fast Multipole Boundary Element Method (FMBEM) and a computer code for 3D elasticity is developed. Higher order boundary elements with quadratic shape functions, i.e. 8-node Serendipity elements, are applied to the discretization of geometry and boundary quantities. The numerical integration of boundary integrals, depending on Kelvin solutions, involves an adaptive subdivision of elements to provide a high accuracy of the calculations. The efficiency of the method is evaluated in terms of the model size, accuracy and execution time by a comparison with Finite Element Method (FEM) models, with quadratic shape function elements. Models of selected machine components, with stress concentration, are analysed. For the analysed structures, both methods provide results with similar accuracy. However, the FMBEM models have by an order of magnitude lower number of Degrees of Freedom (DOF) compared to the FEM, and can be analysed within time comparable to the FEM with a direct solver. Thus, the FMBEM can be competetive to the widely used FEM.

1 INTRODUCTION

The main advantage of the BEM is that in basic problems, for instance linear elasticity, it only requires the discretization of the boundary [2, 3, 7, 5, 8, 1]. On the other hand, the matrices arising in the conventional BEM are fully populated and non-symmetric. Therefore, the method is ineffcient in the analysis of structures with more than a few thousands degrees of freedom. In the last two decades, novel versions of the BEM aiming at reducing its computational complexity have been developed. One of them is the fast multipole boundary element method, FMBEM [10, 9], that is based on the fast multipole method (FMM) [6]. Some of available codes implement constant boundary elements that allow to use rapid analytical integration [9]. However, it is known that higher order

boundary elements have advantages over the constant elements. The higher order elements approximate complex geometry more accurately, provide better convergence rate, allow to calculate physical quantities in points near to the boundary more efficiently, and allow to analyse thin-walled structures [15]. In the present FMBEM, Serendipity 8-node boundary elements with adaptive numerical integration described in [1] are applied. The present work is a continuation of [13], where the efficiency of the FMBEM applied to the analysis of structures containing pores was evaluated. In the present work, typical machine components are analysed, namely a connecting rod and a crankshaft.

2 FAST MULTIPOLE BOUNDARY ELEMENT METHOD

The FMBEM system of equations takes the following form [11]:

$$\mathbf{A}^{\text{near}}\mathbf{y} + \mathbf{a}^{\text{far}} = \mathbf{B}^{\text{near}}\mathbf{z} + \mathbf{b}^{\text{far}}, \tag{1}$$

and is solved iteratively, e.g by the GMRES (Generalized Minimal Residual) method. The matrices $\mathbf{A}^{\text{near}}$ and $\mathbf{B}^{\text{near}}$ include the integrals of fundamental solutions calculated directly. They are calculated once and stored in the memory as sparce matrices. The first matrix is utilized in each iteration to compute the near-field elements in the left hand side matrix-vector product. Selected elements of the matrix are used as a preconditioner for the iterative solver. The $\mathbf{a}^{\text{far}}$ and $\mathbf{b}^{\text{far}}$ vectors include the far-field influence that depend on the fundamental solutions and unknown and known boundary quantities respectively. Elements of the vectors are computed by using expansions and translations.

The idea of FMBEM is based on a hierarchical clustering of the collocation points and boundary elements (Figure 1) and a distribution of potentials over the clusters. The clustering process is mapped by a tree structure with the whole domain corresponding to root on level 0 (Figure 2a). Tree nodes at the highest level, that are called leaves, correspond to the smallest clusters. The potentials are integrals depending on the fundamental solutions and boundary displacements and tractions, that occur in the boundary integral equation [1, 9]. This idea is realized by the application of multipole expansions for the far-field potentials. Coefficients of the expansions - multipole moments - are dependent on the quantities related to the clusters of integration points. Centers of the multipole moments are shifted to centers of larger clusters (moment-to-moment translation, M2M) and transformed into moments of a local expansion (moment-to-local translation, M2L). The centers of the local moments are shifted to centers of smaller clusters (local-to-local translation, L2L) and to each collocation point. The expansions are applied to the far-field potentials. The near-field potentials, that involve the influence of the neighbour clusters, are calculated directly as in the conventional BEM. The system of equation is solved iteratively. A single iteration involves the following operations for the calculation of the matrix-vector product:

1. Computation of the near-field potentials by using the coefficients stored in the $\mathbf{A}^{\text{near}}$ matrix, that are calculated directly.

2. Calculation of the multipole moments for leaves.

3. M2M translations with the upward pass.

4. M2L translations.

5. L2L translations with the downward pass.

6. Calculation of the far-field potentials by using the local series.

In the parallel computations, the tree structure is partitioned in order to define tasks that are assigned to threads. The partitioning is realized by two lists, that are built for each thread, that contain a range of nodes at which the above operations are initialized. In particular, the operations (1), (2), (3) and (6) are initialized using a list that contains a range of the leaves (List 1 in Figure 2). Operations (4) and (5) are initialized using List 2 that contains a range of nodes on the level 2. More details on the algorithm and developed code can be found in papers [11, 12, 13].

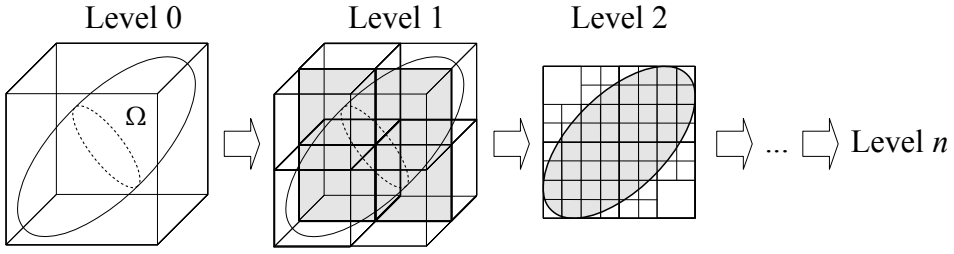

Figure 1: Clustering boundary elements and nodes

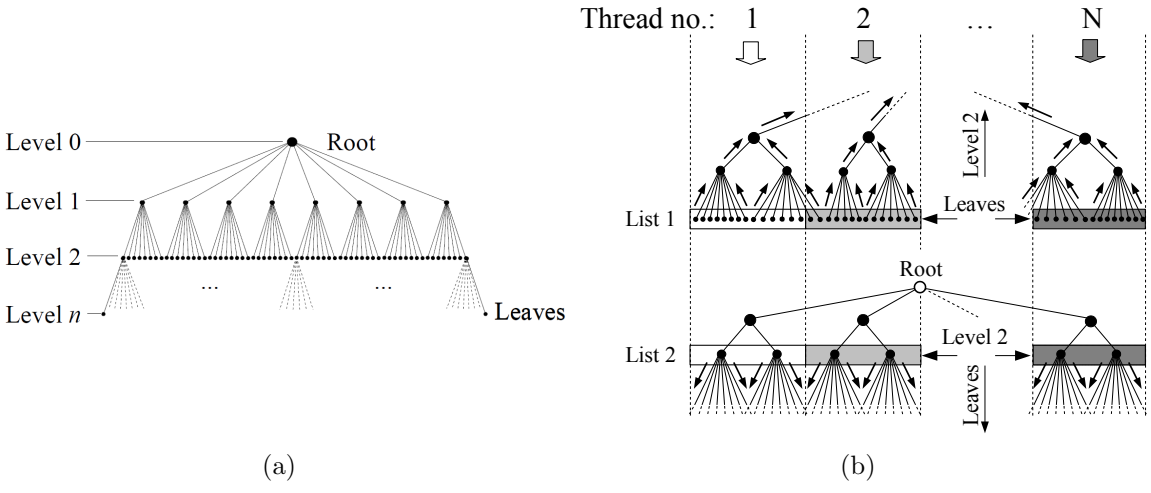

Figure 2: Multipole tree: a) a clustering result, b) parallel computations

3 NUMERICAL EXAMPLES

3.1 Connecting rod

A model of connecting rod is analysed. Material parameters correspond to steel in the temperature of 100°C: Young's modulus $E = 205$ GPa and shear modulus $G = 78$ GPa. Main dimensions of the part and boundary conditions are shown in Figure 3. The inner diameter of the big end is equal to 45 mm, and the small end inner diameter equals 24 mm. The distance between bearing axes equals 132 mm. The height of both ends equals 24 mm. The inner face of the small end is clamped. To the inner face of the big end, a traction force t_n corresponding to a bearing load is imposed. The force acts in the direction normal to the face on the part of total angle 120°, and its value is $t_n = 26$ MPa.

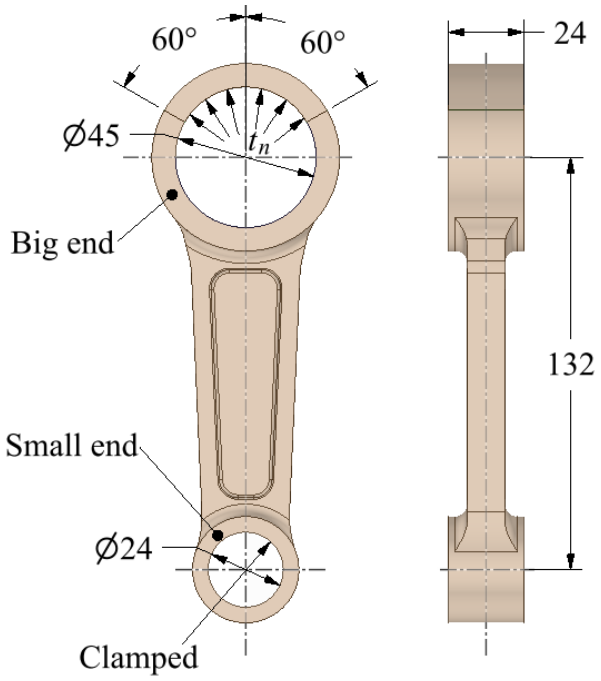

Figure 3: Selected dimensions and boundary conditions applied to the rod model

Three FEM models, with increasing density of the finite element mesh, are developed to achieve convergence of the stress results within the tolerance of 1%. The models are denoted by FEM-1, FEM-2 and FEM-3 respectively. 10-node tetrahedral elements with quadratic shape functions are used. To assess the mesh quality, an error in geometry approximation d_V is introduced. The error is defined as:

$$d_V = \frac{|V^D - V|}{V} \cdot 100\%, \tag{2}$$

where V is the volume of the original model and V^D is the volume of the discretized geometry. Number of elements, nodes, total number of degrees of freedom (DOF) and the

error in geometry approximation are listed in Table 1. An FMBEM model is developed and corresponding parameters are given in the table. 8-node Serendipity elements with adaptive integration are used. Expansions of order $p = 15$ are applied. The GMRES tolerance is set to 10^{-4}. The maximum level of the tree is set to 4. Discretized FEM and FMBEM models are shown in Figure 4. Displacement and stress results for all models are shown in Table 2. Displacement and stress distribution maps obtained by FEM-3 and FMBEM models are shown in Figures 5 and 6 respectively.

Table 1: Details of the discretized models

Model	No. of elements	No. of nodes	Total no. of DOF	d_V, %
FEM-1	30 549	49 255	147 765	0.028
FEM-2	107 914	169 765	509 295	0.009
FEM-3	226 654	350 531	1 051 593	0.006
FMBEM	13 009	4 337	39 024	0.002

The FMBEM model number of DOF is of the order 10^4 while for the FEM models the order ranges from 10^5 to 10^6. The FMBEM provides better approximation of geometry than the finest FEM model (Table 1). The FMBEM displacement and stress values are within the tolerance of 1% with respect to the converged FEM results (Table 2).

The execution time is investigated. The calculations are performed by using a PC with the Intel Xeon CPU E3-1246 v3, 3.50 GHz clock. For both FEM and FMBEM, 8 threads are used. For FEM (MSC Patran/Nastran), the calulations are performed by using default direct and iterative solvers. The execution time for each model is shown in Table 2. The FMBEM time is longer than the FEM-1 and FEM-2 time, and is shorter than the FEM-3 time. The FMBEM time is close to the FEM-1 time and the direct solver.

Table 2: Resultant displacement u, Huber-von Mises stress σ_{red} and execution time

Model	$\max(u)$, mm	$\max(\sigma_{\text{red}})$, MPa	Direct solver, s	Iterative solver, s
FEM-1	0.1798	401.3	265	29
FEM-2	0.1804	401.9	168	162
FEM-3	0.1804	400.9	516	437
FMBEM	0.1795	401.8	–	272

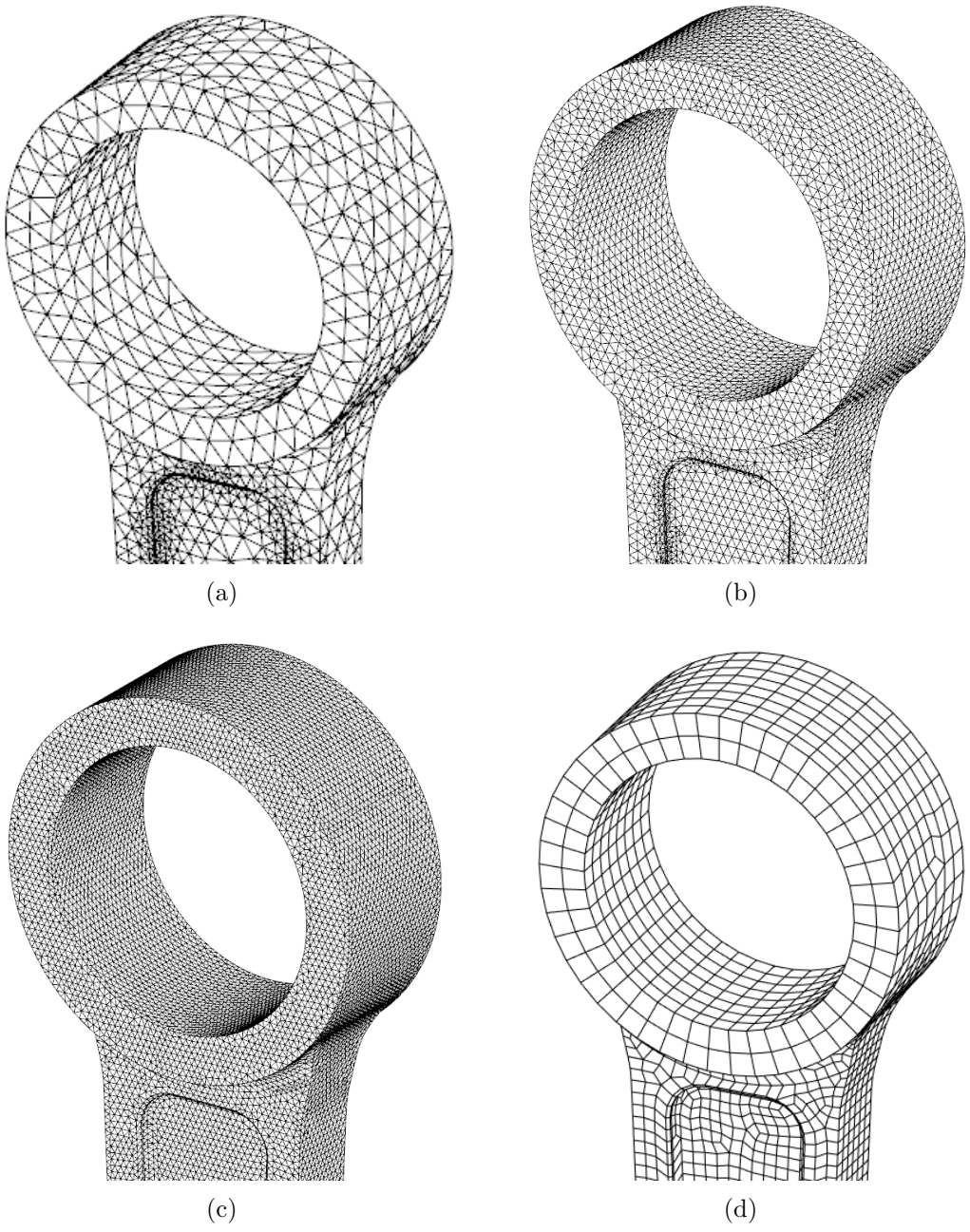

Figure 4: Part of the discretized model: a) FEM-1, b) FEM-2, c) FEM-3, d) FMBEM

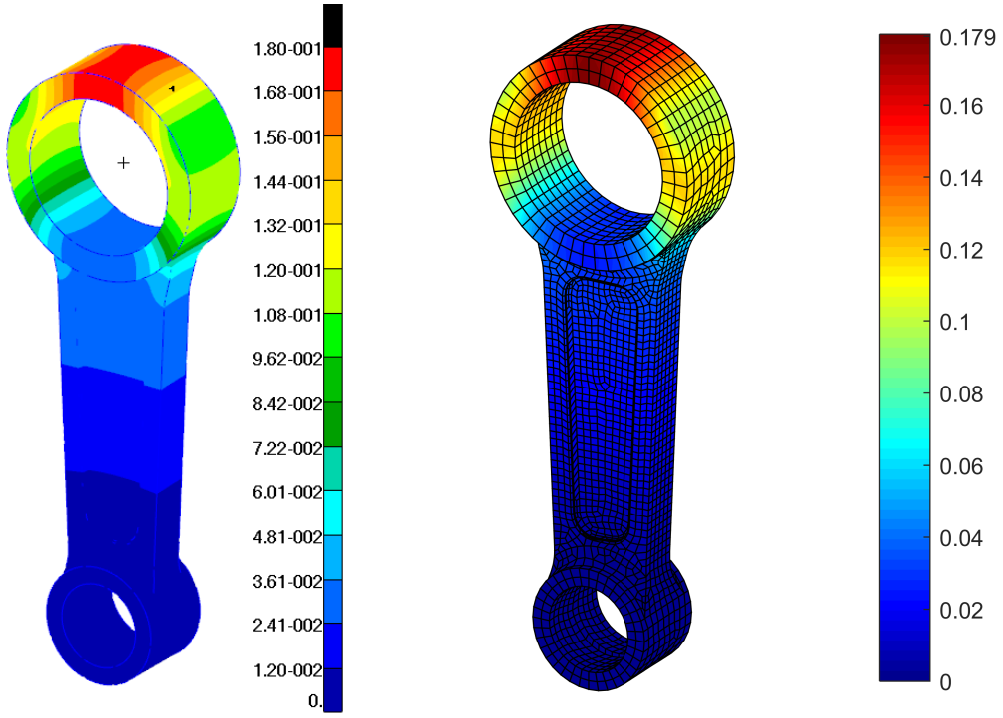

(a) (b)

Figure 5: Resultant displacement (mm): a) FEM-3, b) FMBEM

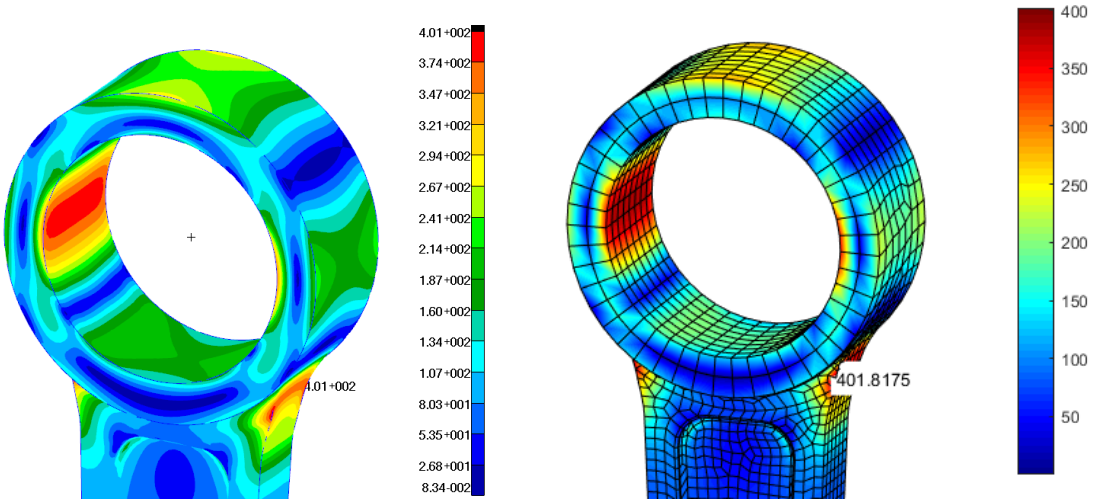

(a) (b)

Figure 6: Reduced Huber-von Mises stress, MPa: a) FEM-3, b) FMBEM

3.2 Crankshaft

Stress distribution in a crankshaft model is analysed by FEM and FMBEM. Geometry of the model with main dimension is shown in Figure 7. Material parameters correspond to steel: Young's modulus $E = 200$ GPa and Poisson's ratio $\nu = 0.3$. Boundary conditions are shown in Figure 8. On faces A and D, displacements in x and y directions are equal to zero. On face C, displacement in z direction is equal to zero. On face B, a traction force corresponding to action of a rod is imposed. The traction force acts in the normal direction, on a part of the face corresponding to angle 120°. Its value is $t_n = 10.1$ MPa. The resultant force is rotated by 9° with respect to y axis and causes bending and torsion of the crankshaft (Figure 8b).

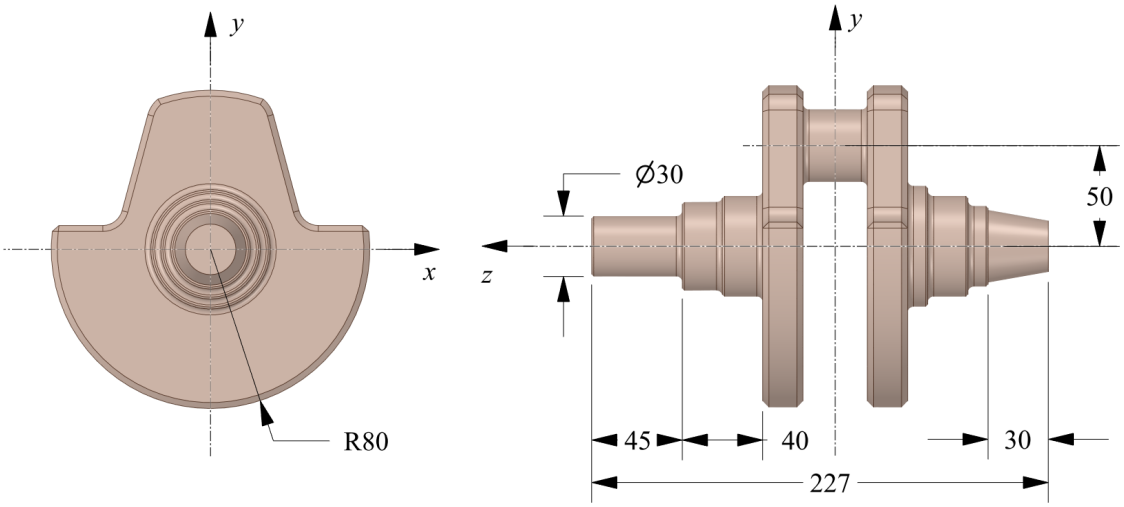

Figure 7: Crankshaft selected dimensions

An FEM model is developed, by using 10-node tetrahedral elements with quadratic shape functions. The measure of the mesh quality is computed as defined by Equation (2). The same structure is modeled by the FMBEM with 8-node Serendipity elements. Parameters of the finite and boundary element meshes are given in Table 3. Detailed view on the stress concentration region discretized by the finite and boundary elements is shown in Figures 9a and 9b respectively. For the FMBEM, the expansion degree is set to 15, the GMRES tolerance is 10^{-5} and maximum tree level is 5.

Table 3: Details of the discretized models

Model	No. of elements	No. of nodes	Total no. of DOF	d_V, %
FEM	569 348	869 429	2 608 287	$4 \cdot 10^{-4}$
FMBEM	29 949	89 849	269 547	$6 \cdot 10^{-4}$

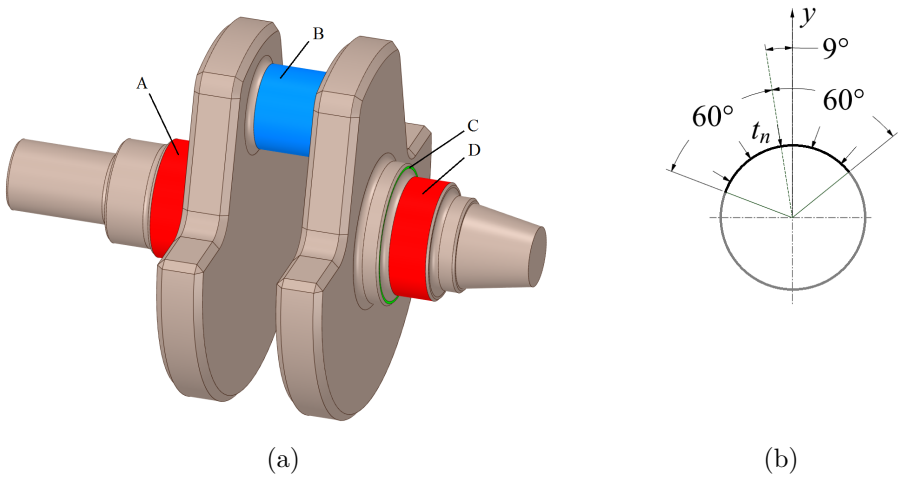

(a) (b)

Figure 8: Crankshaft boundary conditions: a) A: $u_x, u_y = 0$; B: $t = t_n$; C: $u_z = 0$; D: $u_x, u_y = 0$; b) xy plane section of surface B with the normal traction force t_n

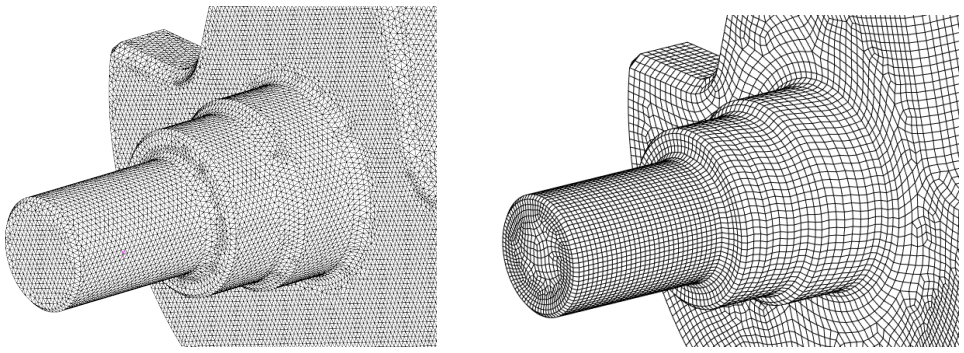

(a) (b)

Figure 9: Detailed view of the element mesh in the stress concentration region: A) FEM, B) FMBEM

The stress distribution in the crankshaft is analysed (Figure 10). The maximum Huber-von Mises stress values, with the execution time, are listed in Table 4. For the calculations, the same computer is applied as for the previous example. Although both the discretized models approximate the geometry very accurately, the maximum stress calculated by the FMBEM is by 10 % higher with respect to FEM. The difference is caused by a stronger stress concentration than that of the previous example. The finite element mesh applied here is a result of some preliminary research that provided only the FEM convergence of the stress result within the tolerance of about 4%. The preliminary research is not presented here due to the article length limitation. The FMBEM result is higher and more safe. On the other hand, the FMBEM execution time is longer that that of FEM with the direct solver, by about 15%. Still, the time is comparable to FEM.

Table 4: Huber-von Mises stress σ_{red} and execution time

Model	max(σ_{red}), MPa	Direct solver, s	Iterative solver, s
FEM	50.59	2 337	787
FMBEM	56.52	–	2 701

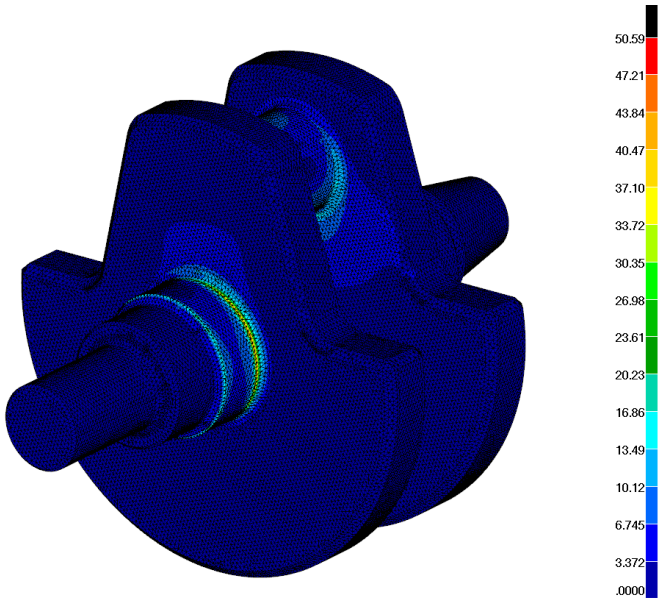

(a)

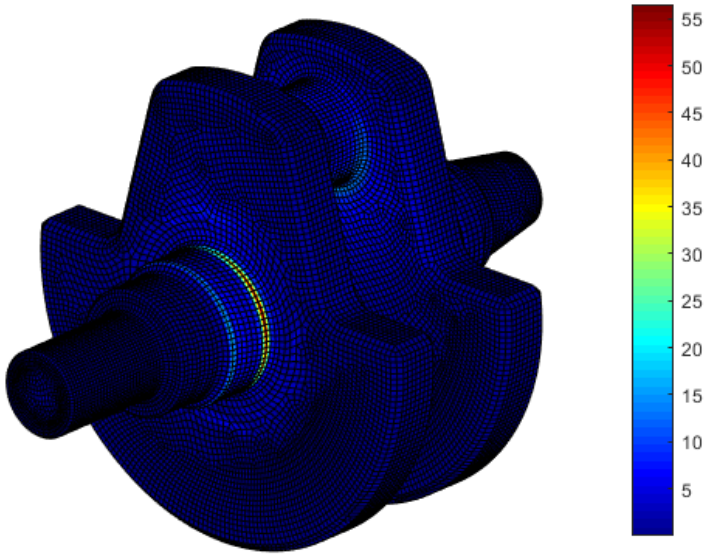

(b)

Figure 10: Huber-von Mises stress, MPa: A) FEM, B) FMBEM

4 CONCLUSIONS

- The efficiency of the Fast Multipole Boundary Element Method for 3D elasticity, with 8-node Serendipity elements and adaptive integration is evaluated. The evaluation is performed by a comparison with the Finite Element Method (FEM) MSC.Patran Nastran commercial code, with default direct and iterative solvers. The efficiency measures include model size, error in geometry approximation and the execution time. The error in geometry approximation is defined as relative difference between the volume of the original and discretized model.

- Models of typical machine parts are analysed: a connecting rod and a crankshaft. The FEM model number of degrees of freedom (DOF) ranges from the order of 10^5 to 10^6. The size of corresponding FMBEM models is in the order of 10^4 to 10^5 respectively. All models approximate the geometry with the error of 0.03% or lower.

- The FMBEM provides displacement and stress results within the tolerance of 1% with respect to the converged FEM results obtained for the connecting rod model. For the crankshaft with a high stress concentration, the FMBEM maximum stress result is by about 10% higher than corresponding FEM value. The FMBEM execution time is close to the FEM with the direct solver.

- 3D linear elastic structures can be modeled by the present FMBEM with by an order of magnitude less DOF, comparable accuracy and time close to the FEM with the direct solver. The reduced number of DOF simplifies the preprocessing stage and reduces the amount of postprocessed data. Thus, the FMBEM can be competetive to the widely used FEM.

- The FMBEM execution time can be reduced, e.g. by the application of an optimized M2L translation, GPU calculations [14], balanced multipole tree [4] and possibly other improvements.

Acknowledgments The scientific research was funded by National Science Centre, Poland, grant no. 2017/01/X/ST8/00376.

REFERENCES

[1] Beer, I., Smith, I. and Duenser, C. *The boundary element method with programming for engineers ans scientists*. Springer, (2008).

[2] Brebbia, C. A. and Dominguez, J. *Boundary elements an introductory course*. McGraw–Hill, (1992).

[3] Burczyński, T. *Boundary element method in mechanics* Scientific and Technical Publishing WNT, (1995), in Polish.

[4] Engblom, S. On well-separated sets and fast multipole methods, *Appl. Numer. Math.* (2011), **61**, 10, pp. 1096-1102.

[5] Gao, X. W. and Davies, T. G. *Boundary element programming in mechanics*, Cambridge University Press, (2002).

[6] Greengard, L. and Rokhlin, V. A fast algorithm for particle simulations, *J. Comput. Phys.* (1987),**73**, pp. 325-348.

[7] Kane, J. H. *Boundary element analysis in engineering continuum mechanics*, Prentice-Hall, (1994).

[8] Linkov, A. M. *Boundary Integral Equations in Elasticity Theory*, Kluwer Academic Publishers, (2002).

[9] Liu, Y. *Fast multipole boundary element method Theory and applications in engineering*. Cambridge University Press, (2009).

[10] Nishimura, N. Fast multipole accelerated boundary integral equation methods, *Appl. Mech. Rev.* (2002), **55**, pp. 299-324.

[11] Ptaszny, J. Accuracy of the fast multipole boundary element method with quadratic elements in the analysis of 3D porous structures, *Comput. Mech.* (2015) **56**, pp. 477–490.

[12] Ptaszny, J. Parallel fast multipole boundary element method applied to computational homogenization, *AIP Conference Proceedings* (2018) **1922**, 140003.

[13] Ptaszny, J. and Hatłas, M. Evaluation of the FMBEM efficiency in the analysis of porous structures, *Eng. Computation.* (2018) **35**, DOI: 10.1108/EC-12-2016-0436.

[14] Wang, Y., Wang, Q., Deng, X., Xia, Z., Yan, J. and Xu, H., Graphics processing unit (GPU) accelerated fast multipole BEM with level-skip M2L for 3D elasticity problems, *Adv Eng Software* (2015) 82, pp.105–118.

[15] Zhang, Y., Li, X., Sladek, V., Sladek, J. and Gao, X. Computation of nearly singular integrals in 3D BEM, *Eng. Anal. Bound. Elem.* (2014) **48**, pp. 32-42.